FABRICATION OF HOLLOW COMPOSITE STRUCTURE MICROFLUIDIC DOUBLE-END CLAMPED BEAM

Jingjing WANG, Baozheng XU

Tiangong University, School of Electronic and Information Engineering, Tianjin 300380, China
Corresponding author: Jingjing WANG, E-mail: `jingjingwang@tiangong.edu.cn`

Abstract. Double-end clamped beam is one of the most important miniaturized structures in micro-electromechanical systems (MEMS). In recent years, they have achieved extensive application in a variety of fields, including environmental monitoring, food detection, and disease diagnosis, since they have high sensitivity, high throughput, good specification and fast response. To meet the market demand for precise three-dimensional microstructures and tiny device sizes, the rationalization of the process design of micro-nano technology is essential. In previous research, the function of the microcantilever sensor was finally realized through eight lithography cycles. High performance piezoresistive microcantilever arrays were successfully developed with a yield of 90% in our work. In this paper, a hollow composite microfluidic double-end clamped beam structure is proposed, a reasonable process flow is developed. Simulations show that the hollow microfluidic structure's sensitivity can reach the order of 10^{-12} g, and the quality factor is nearly stable above 10,000. It is crucial for the development of double-end clamped beam sensors because it offers a low-cost, portable, and rapid detection method for the detection of biomolecules.

Key words: double-end clamped beam, microfluidic, process, photolithography.
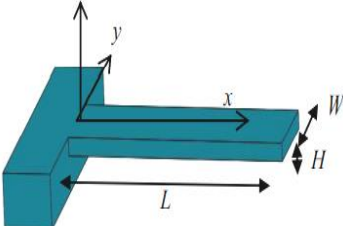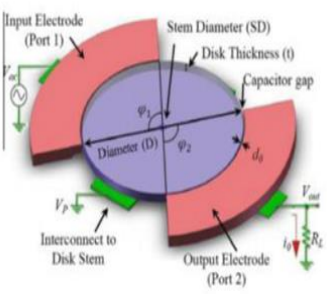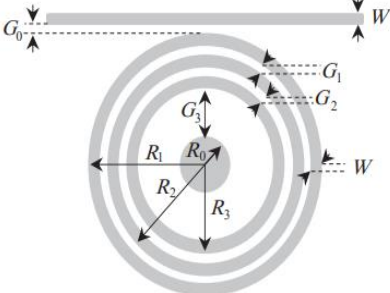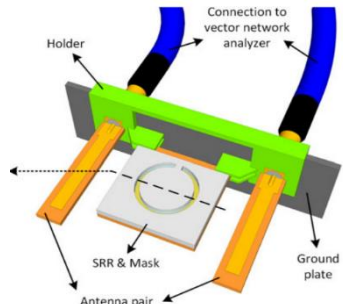
1. INTRODUCTION

With the cross-fusion of electronic information science and biotechnology technology, microelectromechanical systems technology and nanotechnology, various novel micro and nano sensors have been developed [1]. MEMS sensors as a significant application in the field of biochemical information detection, they have a wide application in healthcare, life sciences and agricultural science instrumentation, etc. [2].

Three types of sensors are capable of applying in aqueous media: optical sensors, electrochemical sensors and mass-sensitive sensors. Optical sensors are fast, sensitive, and perform good advantages in in-situ sensing and real-time detection. However, the sophisticated system and the intricacy detection method making it difficult to achieve batch production and widespread application [3]. Electrochemical sensors have the advantages of miniaturization, low-cost, high sensitivity, and independence from solution turbidity [4]. However, the sensor is affected by external environment (such as temperature, humidity, and pressure) and has poor stability. Four primary structures of mass-sensitive sensors based on resonant structures in microelectromechanical systems (MEMS) are beams [5], discs [6], rings [7], and interdigitated structures [8], as shown in Table 1.

The microbeam structure has the advantages of small size, simple structure, high sensitivity, and easy arraying and integration [9], which becomes the most promising devices in the field of detection of molecular dynamics characteristics [10].

Compared with cantilever, double-ended clamped beams offer more stability and resonance frequencies, making them ideal to application as a biosensor.

Table 1

Comparison of various structural sensors

Structure	Schematic	Features	Application
Beam [5]		Small size, Simple structure, High sensitivity, Easy to array and integrate	Medical testing, Life health, Agricultural Production
Disc [6]		High sensitivity, Strong detection ability, Small dynamic range, Complex	Chemical analysis, Biomonitoring
Ring [7]		High sensitivity, Small size, High cost	Optical detection
Interdigitate [8]		Low cost, High portability, Volatile structure,	Detection of blood indicators

Double-ended clamped beam biosensors detect target analytes with biological reactions. And they are mainly used for mass or concentration detection of tiny particles of analytes in chemistry detection. Currently, microbeam sensors for liquid biochemical molecule detection have focused on the following two approaches: High quality factor(Q) and high sensitivity. The majority of biological detection for cancer cells, markers, DNA, etc. is concentrated on drying after the liquid reaction is finished, which cannot achieve in situ real-time detection in a liquid environment. This technique reduces microbial activity after drying and decreases detection accuracy. Erman Timur Dogan et al. from KOC University proposed a flow cell for antigen-antibody reaction detection in real time [11], although this approach can achieve in situ real-time detection of biochemical molecules, the microbeam is affected by damping in a liquid detection environment, and the Q decreases sharply (below 10^2), which makes the detection sensitivity decrease dramatically [12].

The rapid development of microfluidic devices based on the concept of the flow cell [13] due to the current demand for high Q and high sensitivity in biosensors. Microfluidic encapsulation shells made of polydimethylsiloxane (PDMS) have been used in microbeam biosensors published in recent years. Although integrating microfluidics and microcantilever beams overcomes both real-time monitoring and bioactivity challenges, the majority of these microfluidic systems are still based on beam arrays, which have low binding efficiency and high sample consumption.

A novel structure of double-ended clamped beam biosensor was proposed. By investigating the advantages of high sensitivity of micro-beam structures in vacuum and the characteristics of microfluidic in-situ real-time monitoring in liquid samples, this structure integrates the microfluidic channel inside the resonant beam.

The target molecule is absorbed when the solution is introduced inside the double-end clamped beam; the vibration frequency of the whole double-end clamped beam is detected in vacuum. The piezoresistive structure at the clamped end detects the frequency shift of the double-ended beam during the reaction in real time.

This new resonant composite beam array biosensor is fabricated by MEMS micro and nano processing technology, which can realize the effective isolation of the immune reaction environment from the double-end clamped detection environment and high-sensitivity, in situ real-time rapid detection of analyte.

2. STRUCTURAL DESIGN

Based on double end clamped beam structure model, the hollow composite double-end fixed beam structure has been developed with a local reaction cavity that can effectively reduce the effecttion on the stiffness coefficient during the reaction. To raising the detection limit of double end fixed beam, pillar arrays were fabricated on local reaction cavity, and the model is shown in Fig. 1. The length of beam is 200 μm, width of beam is 50 μm, the thickness of beam is 5 μm, and the local reaction cavity in the middle of beam.
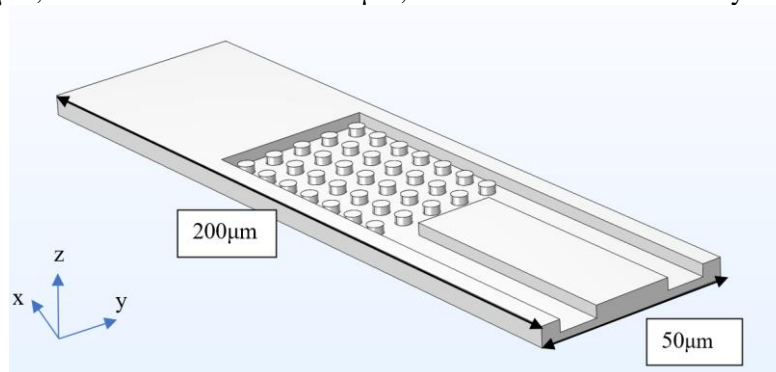

Fig. 1 – Double end clamped beam structure with local reaction cavity

The reaction area is increased by 25% when 35 pillar arrays with a radius of 2 μm and a height of 4 μm are added internally. Additionally, the upper surface of the structure is made of a flexible material in order to effectively separate the reaction environment from the detection environment and enhance the double end clamped beam's detection reliability. Analytes are added to the reaction chamber through a microfluidic system where the effects of the external environment are effectively controlled.

Simulation experiments were conducted on the double end clamped beam with a reactive cavity structure, and the simulation results showed that the stability of the structure was unsatisfactory, and the vibration mismatch occurred. The mismatch cannot be eliminated by changing various dimensions of the device. there is a significant elastic mismatch between the two parts due to differences in the Young's modulus of the flexible material and the substrate silicon. The structural material was optimized. The flexible material on the upper surface was substituted with silicon nitride. Finally, the vibration mismatch was eliminated.

The hollow composite structure of the microfluidic double end clamped beam is designed as shown in Fig. 2. The whole structure is divided into two major parts: the bottom substrate and the upper microfluidic channel. The analyte can be introduced into the microfluidic channel from the inlet port during the reaction and remove the waste liquid from the outlet port when the detection is finished, which will prevent cross-

infection of the device. The combination of multiple double-end clamped beam structures is beneficial to the joint detection of the analyte. The bottom substrate of the structure is made of silicon material and the microfluidic structure is made of silicon nitride. The structural dimensions and sizes of each part are shown in Table 2.
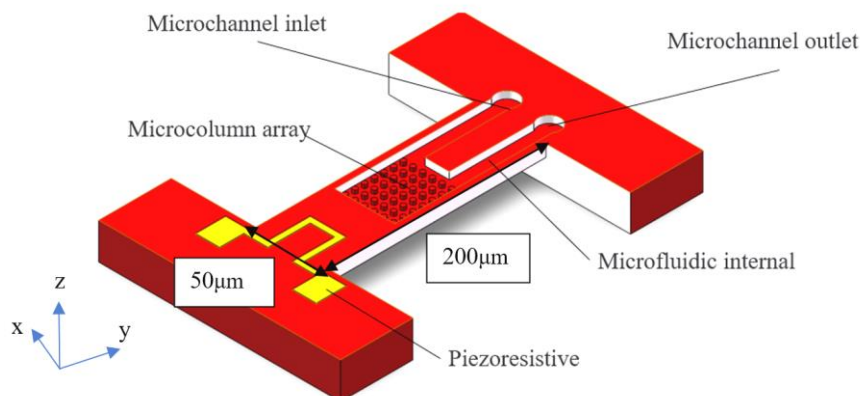

Fig. 2 – Hollow composite structure double-end clamped beam design.

Table 2

Dimensions of hollow microfluidic structures

unit of measurement	size (μm)
beam substrate length	200
beam substrate width	50
beam substrate thickness	5
beam channel wall thickness	4
beam channel sidewall length	150
beam channel width	10
reaction chamber width	40
microcolumn size	$r = 2$, $h = 4$

3. FABRICATION PROCESSES OF DOUBLE END CLAMPED BEAM

The design of the process flow for the silicon-based double-end clamped beam is shown in Fig.3. The 4-inch SOI wafer was used, thickness of device layer is 5 μm, buried oxygen layer is 1 μm, and handle layer is 400~450 μm. The BOX (Buried Oxide) layer, which divides the device layer from the handle layer enhanced efficiency and lower process variation, effectively safeguards the device layer.

The Wheatstone bridge's electrical circuits and piezoresistive structure were firstly generated utilizing two different ion implantation techniques, respectively. Next, the microfluidic channel and local reaction cavity of the double-end clamped beam were fabricated by inductively coupled plasma etching (ICP). Subsequently, the beam structure was formed by reaction ion etching (RIE). The surplus metal on the photoresist was then removed by lift-off to generate a metal electrode pad after Cr/Au evaporation. As a sacrifice layer, a layer of SiO_2 is deposited using (plasma enhanced chemical vapor deposition) PECVD on the reaction cavity and microfluidic channel. Next, a layer of silicon nitride is deposited by PECVD to generate the composite hollow channel structure. The bulk silicon is then etched within 350 μm depth by deep reaction ionetching (DRIE), and then aluminum was evaporated by electron-beam evaporation using as a cut-off layer for isotropic etching. Thereafter, the remain bulk silicon is removed using an isotropic etching method to generate a resonant cavity. Finally, the beam and hollow channel structure is released using a wet etching technique.
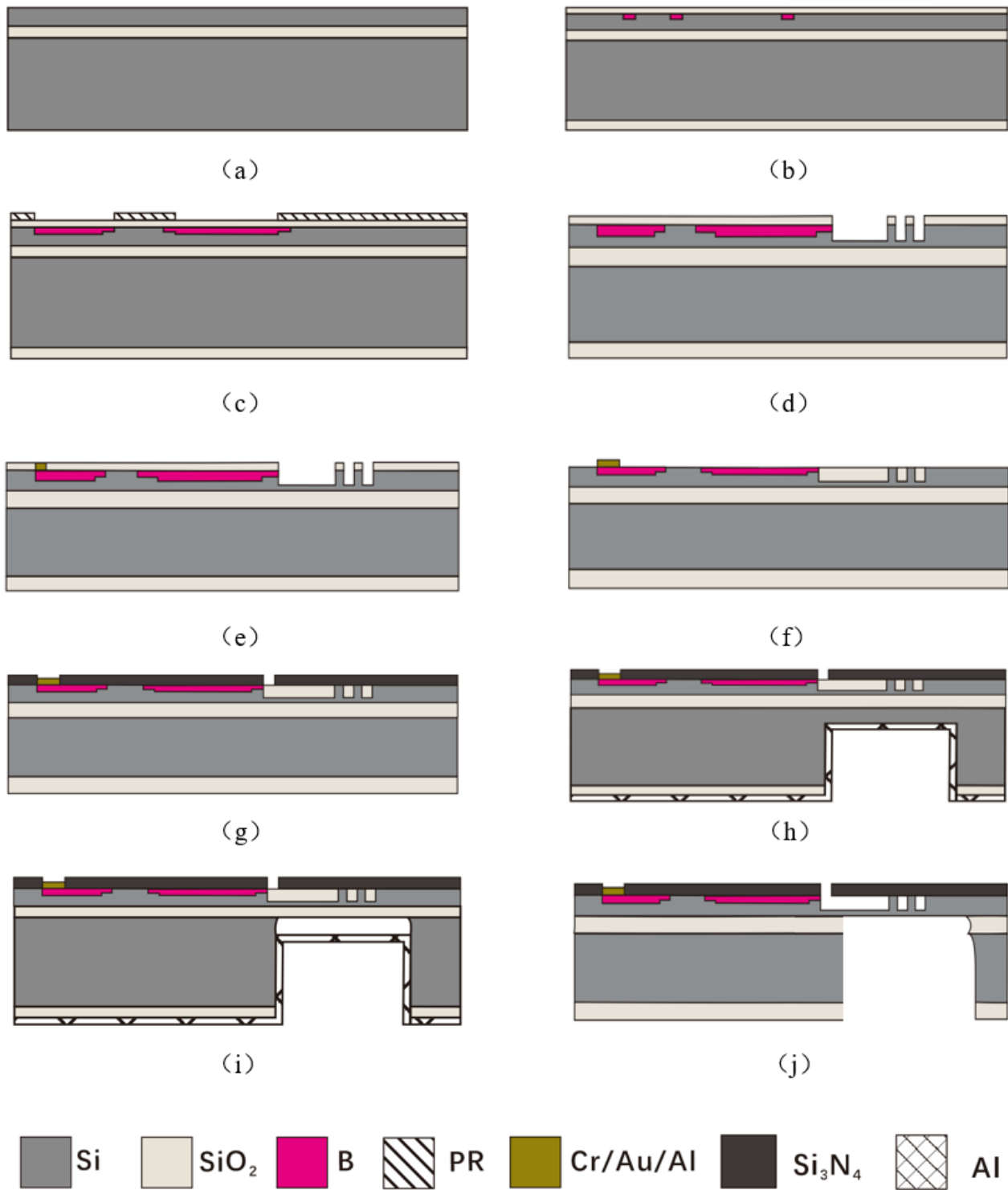
Fig. 3 – Process flow design of double end clamped beam: a) SOI wafer; b) ion implantation; c) photoetching; d) etching; e) Cr/Au evaporation; f) metal lift-off; g) PECVD; h) al evaporation; i) etching; j) beam release.

The first lithography as well as ion implantation is performed first. The resulting piezoresistive pattern is shown in the Fig. 4.

Ion injection was intended to generate an electrical transmission line for high-energy ion injection after the second lithography, with injection of Boron ion. Injection energy was 100 keV, and injection dose of 9 E15 cm^{-2}.

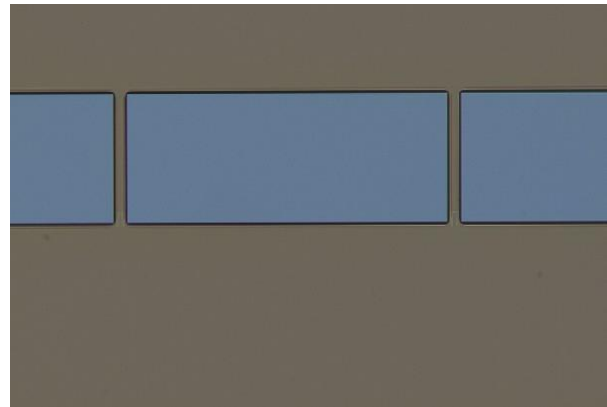Fig. 4 – Piezoresistive formation by ion injection.

Fig. 5 – ICP etching to generate a double end clamped beam structure.

Next, the structure of the double end clamped beam was fabricated, the equipment is Oxford ICP etching, as shown in the Fig. 5.

The layer of gold was vaporized on the pad of the transmission line, as shown in Fig. 6a to facilitate the signal of readout. The instrument quasi-probe tests the resistance of the ion injection transmission line was measured to be about $3 \, k\Omega$, as shown in Fig. 6b. The linear relationship between voltage and current demonstrates that the metal and silicon maintain an excellent ohmic contact.
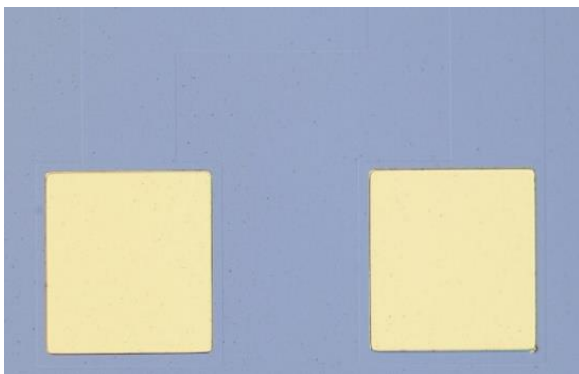
(a) Gold covered on the Pad
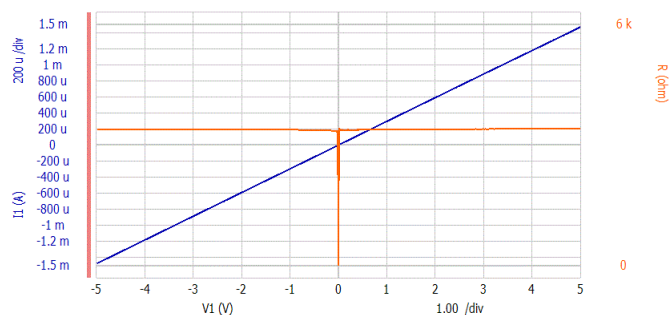
(b) *I-V* curve relationship on the Pad

Fig. 6 – *I-V* curve relationship between metal Pad and Pad on.

The severe unevenness of the back-side etching was resolved by changing the resonant cavity etching step to a two-step combination of back-side anisotropic etching and front-side isotropic etching.

The deep reaction ionetching process was divided into three main parts: Etch A for passivation removal, Etch B for silicon chemical reaction etching, and the final step for sidewall passivation. The depth of the etching within the SOI wafer can be regulated by adjusting the parameters of the first two phases. The chemical equation of the process reaction is as follows：

The distribution of the double-end clamped beam array inside the 4-inch wafer is shown in Fig. 7. The deep etching of the backside bulk silicon using the two-step alternating method of: Etch A electrode power of 600 W, etching time of 1 s and Etch B electrode power of 10 W, etching time of 5 s. After 500 cycles of etching, the distribution of etching depths in the transverse and longitudinal directions within the wafer is shown in Tables 3 and 4. The etching rate is the fastest in the center, where the depth has reached $343 \, \mu m$, while the etching depth in the slowest area at the edge is only $292 \, \mu m$, with a difference of $51 \, \mu m$ and an intra-wafer variation of 8.1%.
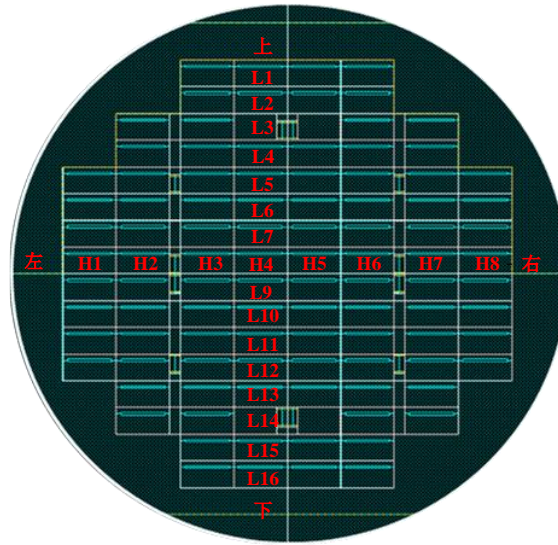
Fig. 7 – Distribution of double-ended solid-supported beam arrays within a SOI wafer.

Table 3

Transverse etching depth distribution at 10 (W)

Distribution	H1	H2	H3	H4	H5	H6	H7	H8
Depth (μm)	309.8	331	340.2	342.8	342.9	340.2	331.3	314.4
Difference	33.1	11.9	2.7	0.1	0	2.7	11.6	28.5
Percentage	5.1%	1.8%	0.4%	0.0%	0.0%	0.4%	1.7%	4.3%

Table 4

Longitudinal etching depth distribution at 10 (W)

Distribution	L1	L2	L5	L8	L9	L12	L15	L16
Depth (μm)	291.9	311.5	337	342.8	343.21	341.3	327.4	315.5
Difference	51.31	31.71	6.21	0.41	0	1.91	15.81	27.71
Percentage	8.1%	4.8%	0.9%	0.1%	0.0%	0.3%	2.4%	4.2%

Etch B maintained the same etching parameters of 10 W and 5 s. The passivate ion etching power of Etch A was increased from the original 600 W to 700 W for 50 etching cycles. The etching rate was rapidly increased from 0.68 μm/loop at 600 W to 0.98 μm/loop, and the in-chip uniformity was significantly improved. The minimum etch depth at the edge was 42.5 μm when etching 48.9 μm depth in the middle region, and the in-wafer variation was reduced to 7.0%.

In summary, the maximum deviation of the in-wafer etching depth was reduced from 14% to within 5% by optimizing the DRIE parameters, and the process parameters for deep back-side etching were determined to be Etch A 700 W, 1.5 s and Etch B 10 W, 5 s.

The alignment precision of the double-sided lithography determines the length of the double-end clamped beam in the fabrication process. Compared to conventional processes, the dimensions of a double-ended clamped beam are determined only by the photolithography and etching process, resulting in improved control of beam dimensional accuracy. According to the proposed process flow and the process parameters, the high-performance piezoresistive microfluidic double-end clamped beam array was fabricated with a high yield rate of 98%.

4. CONCLUSION

In this paper, a novel microfluidic double-ended clamped beam sensor with hollow composite structure is developed, and a reasonable process flow and lithography technique are proposed, and finally the actual processing and fabrication are carried out. To obtain high sensitivity while successfully reducing the dampening effect of the solution on the resonant beam during in-situ detection, microfluidic channels are integrated into the interior of the double-end clamped beam. A complete process flow is defined that requires eight photolithographic realizations to achieve the functionality of a double-ended solid beam sensor with integrated piezoresistive and microfluidic channels. By analyzing the problems in the process, several experiments were carried out on the etching during the fabrication of the double-ended clamped beam. The process parameters are optimized to improve the control accuracy of the double-ended clamped beam dimensions. According to the process flow and corresponding process parameters proposed in this project, it provides guidance for the preparation of high-performance piezoresistive microfluidic double-end clamped beam arrays.

ACKNOWLEDGEMENTS

REFERENCES

1. P. TEERAPANICH, M. PUGNIÈRE, C. HENRIQUET, Y.L. LIN, C.F. CHOU, T. LEÏCHLÉ, *Nanofluidic Fluorescence Microscopy (NFM) for real-time monitoring of protein binding kinetics and affinity studies*, Biosensors and Bioelectronics, **88**, pp. 25–33, 2017.
2. I.B. TAHIRBEGI, J. EHGARTNER, P. SULZER, S. ZIEGER, A. KASJANOW, M. PARADISO, M. STROBL, D. BOUWES, T. MAYR, *Fast pesticide detection inside microfluidic device with integrated optical pH, oxygen sensors and algal fluorescence*, Biosensors and Bioelectronics, **88**, pp. 188–195, 2017.
3. P. MEHROTRA, *Biosensors and their applications – A review*, Journal of Oral Biology and Craniofacial Research, **6**, pp. 153–159, 2016.
4. C. ZHAO, M. M. THUO, X. LIU, *A microfluidic paper-based electrochemical biosensor array for multiplexed detection of metabolic biomarkers*, Science & Technology of Advanced Materials, **14**, *5*, 2013.
5. A. BOISEN, S. DOHN, S.S. KELLER, S. SCHMID, M. TENJE, *Cantilever-like micromechanical sensors*, Reports on Progress in Physics, **74**, art. 036101, 2011.
6. M. OKAN, M. DUMAN, *Functional polymeric nanoparticle decorated microcantilever sensor for specific detection of erythromycin*, Sensors and Actuators B: Chemical, **256**, pp. 325–333, 2018.
7. K. MALMIR, H. HABIBIYAN, H. GHAFOORIFARD, *An ultrasensitive optical label-free polymeric biosensor based on concentric triple microring resonators with a central microdisk resonator*, Optics Communications, **365**, pp. 150–156, 2016.
8. B. CAMLI, E. KUSAKCI, B. LAFCI, S. SALMAN, H. TORUN, A.D. YALCINKAYA, *Cost-effective, microstrip antenna driven ring resonator microwave biosensor for biospecific detection of glucose*, IEEE Journal of Selected Topics in Quantum Electronics, **23**, art. 6900706, 2017.
9. S. PARTEL, S. KASEMANN, V. MATYLITSKAYA, C. THANNER, C. DINCER, G. URBAN, *A simple fabrication process for disposable interdigitated electrode arrays with nanogaps for lab-on-a-chip applications*, Microelectronic Engineering, **173**, pp. 27–32, 2017.
10. S. LEAHY, Y. LAI, *A cantilever biosensor exploiting electrokinetic capture to detect Escherichia coli in real time*, Sensors & Actuators B Chemical, **238**, pp. 292–297, 2017.
11. E. TIMURDOGAN, B.E. ALACA, I.H. KAVAKLI, H. UREY, *MEMS sensor for detection of Hepatitis A and C viruses in serum*, Sensors and Bioelectronics, **28**, *1*, pp. 189–194, 2011.
12. J. TAMAYO, A.D. HUMPHRIS, A.M. MALLOY, M.J. MILES, *Chemical sensors and biosensors in liquid environment based on microcantilevers with amplified quality factor*, Ultramicroscopy, **86**, pp. 167–173, 2001.
13. A. MOUDGIL, K.K. SINGH, S. SWAMINATHAN, *MEMS based design and analysis of a biosensor for detection of hepatitis virus*, IEEE International Conference on Nanotechnology, pp. 805–808, 2015.